

FUSE DETERMINATION OF A LOW DEUTERIUM ABUNDANCE ALONG AN EXTENDED SIGHT LINE IN THE GALACTIC DISK

G. HÉBRARD¹, T. M. TRIPP², P. CHAYER^{3,4}, S. D. FRIEDMAN⁵, J. DUPUIS³,
P. SONNENTRUCKER³, G. M. WILLIGER³, H. W. MOOS³
Draft version December 11, 2018

ABSTRACT

We present a study of the deuterium abundance along the extended sight line toward HD 90087 with the *Far Ultraviolet Spectroscopic Explorer (FUSE)*. HD 90087 is a O9.5III star located in the Galactic disk at a distance of ~ 2.7 kpc away from the Sun. Both in terms of distance and column densities, HD 90087 has the longest and densest sight line observed in the Galactic disk for which a deuterium abundance has been measured from ultraviolet absorption lines so far. Because many interstellar clouds are probed along this sight line, possible variations in the properties of individual clouds should be averaged out. This would yield a deuterium abundance which is characteristic of the interstellar medium on scales larger than the Local Bubble. The *FUSE* spectra of HD 90087 show numerous blended interstellar and stellar features. We have measured interstellar column densities of neutral atoms, ions, and molecules by simultaneously fitting the interstellar absorption lines detected in the different *FUSE* channels. As far as possible, saturated lines were excluded from the fits in order to minimize possible systematic errors. *IUE (International Ultraviolet Explorer)* archival data are also used to measure neutral hydrogen. We report $D/O = (1.7 \pm 0.7) \times 10^{-2}$ and $D/H = (9.8 \pm 3.8) \times 10^{-6}$ (2σ). Our new results confirm that the gas-phase deuterium abundance in the distant interstellar medium is significantly lower than the one measured within the Local Bubble. We supplement our study with a revision of the oxygen abundance toward Feige 110, a moderately distant (~ 200 pc) sdOB star, located ~ 150 pc below the Galactic plane. Excluding saturated lines from the fits of the *FUSE* spectra is critical; this led us to derive an O I column density about two times larger than the one previously reported for Feige 110. The corresponding updated D/O ratio on this sight line is $D/O = (2.6 \pm 1.0) \times 10^{-2}$ (2σ), which is lower than the one measured within the Local Bubble. The dataset available now outside the Local Bubble, which is based primarily on *FUSE* measurements, shows a contrast between the constancy of D/O and the variability of D/H. As oxygen is considered to be a good proxy for hydrogen within the interstellar medium, this discrepancy is puzzling.

Subject headings: ISM: abundances – ISM: clouds – cosmology: observations – ultraviolet: ISM – stars: individual (HD90087) – stars: individual (Feige110)

1. INTRODUCTION

Deuterium, which is produced during primordial nucleosynthesis and then destroyed by astration, is a key element in cosmology. Whereas measurements in low-metallicity QSO absorption systems probe D/H at look-back times of ~ 13 – 14 Gyrs, the present epoch deuterium abundance $(D/H)_{PE}$ can be measured in the interstellar medium (ISM).

The *FUSE (Far Ultraviolet Spectroscopic Explorer)* mission has brought significant progress on the $(D/H)_{ISM}$ measurement. D/H likely has a single value in the Local Bubble⁶, in the range $(1.3$ – $1.5) \times 10^{-5}$ (Moos et al. 2002; Hébrard & Moos 2003). However, it now appears that this local abundance should not be considered as a canonical value characteristic of the Milky Way at the present epoch, as it was usually believed before *FUSE* studies. Indeed, numerous distant sight lines, i.e. sight lines probing

the interstellar medium beyond the Local Bubble, have shown deuterium abundances in disagreement with the Local Bubble one (see, e.g. Laurent et al. 1979, Jenkins et al. 1999, Lemoine et al. 1999, Sonneborn et al. 2000, Hoopes et al. 2003).

Hébrard & Moos (2003) reported a trend in the deuterium abundance based on D/O, D/N, and previously reported D/H measurements: the deuterium abundance is lower than in the Local Bubble for the most distant sight lines exhibiting the highest hydrogen column densities. More recent work by Wood et al. (2004) confirms this low value. These results suggest that the deuterium abundance might be locally abnormally higher than the present epoch value. While Hébrard & Moos (2003) suggested that the present epoch ratio $(D/H)_{PE}$ would be significantly lower than 1×10^{-5} , Linsky et al. (2005) recently proposed a $(D/H)_{PE}$ ratio higher than 2×10^{-5} assuming that deuterium could be significantly depleted onto dust

¹ Institut d’Astrophysique de Paris, UMR7095 CNRS, Université Pierre & Marie Curie, 98^{bis} boulevard Arago, F-75014 Paris, France; hebrard@iap.fr.

² Department of Astronomy, University of Massachusetts, Amherst, MA 01003, USA.

³ Department of Physics & Astronomy, The Johns Hopkins University, Baltimore, MD 21218, USA.

⁴ Department of Physics & Astronomy, University of Victoria, P.O. Box 3055, Victoria, BC V8W 3P6, Canada.

⁵ Space Telescope Science Institute, 3700 San Martin Drive, Baltimore, MD 21218, USA.

⁶ The Local Bubble is a ~ 100 pc-size low-density cavity in which the Solar System is embedded (see, i.e., Sfeir et al. 1999)

grains (see Jura 1982; Wood et al. 2004; Draine 2004).

Both $(D/H)_{PE}$ values may challenge deuterium evolution models, the baryonic density of the Universe inferred from primordial D/H measurements, and our understanding of the physics of the interstellar medium. Regardless of the actual scenario, it is now clear that local measurements are not enough to assess $(D/H)_{PE}$, and that deuterium studies in the distant interstellar medium are mandatory. Only a few are available now.

Here we report the measurement of the deuterium abundance in the interstellar medium toward HD 90087 (§ 2). This sight line is studied thanks to new *FUSE* observations of this target. *IUE* (*International Ultraviolet Explorer*) archival spectra are also used to constrain the neutral hydrogen column density from the fits of the Ly- α line wings. Both in terms of distance and column densities, HD 90087 provides the farthest Galactic line of sight for which deuterium abundance has been measured from far ultraviolet absorption lines to date. Hence, many interstellar clouds are probed along this sight line. This will tend to average out the peculiarities of individual Galactic regions, such as the Local Bubble, in order to reach measurements that are characteristic of the interstellar medium on large scales.

We supplement our study with a reconsideration of the O I column density measurement toward Feige110 from *FUSE* spectra, allowing an updated interstellar D/O measurement on this sight line (§ 3).

2. THE HD 90087 LINE OF SIGHT

2.1. The target

HD 90087 is a bright O-type star located in the fourth quadrant of the Galactic plane. It was assigned different spectral types and luminosity classes in the past, ranging from O9 to B3 and from II to V. The most recent classification is the one given by Mathys (1988): O9.5III. Savage, Meade, & Sembach (2001) reported the spectroscopic parallax distance $d = 2740$ pc, with an accuracy estimated to be about 30 % (i.e. about 800 pc here). This value is in good agreement with the one reported by Diplas & Savage (1994), $d = 2716$ pc. Table 1 summarizes relevant sight line and atmospheric parameters for HD 90087. This target is well beyond the Local Bubble. The column densities that we report below for HD 90087 represent 50-100 times the column densities usually measured within the Local Bubble (e.g., Moos et al. 2002). The interstellar matter located within the Local Bubble is a negligible fraction of the total column of material probed along this sight line, which is dominated by the distant interstellar medium.

2.2. Observations and data processing

The target was first observed with *FUSE* using the low-resolution (LWRS) aperture in April 2000 as a part of a wide study of the hot gas in the Milky Way through the O VI doublet observations (Bowen et al. 2004). Several D I interstellar absorption lines were detected against the stellar continuum on this 3.9 ksec snapshot observation. This indicated that the target is well-suited for distant deuterium abundance measurement. So, an additional 14 ksec observation was performed in June 2003 through the medium-resolution (MDRS) aperture, allowing higher signal-to-noise ratio to be reached and reducing interference from geocoronal emission from the terrestrial atmo-

sphere. The analysis presented below uses both the LWRS and MDRS data. The two observations were obtained in histogram *FUSE* mode. The observing log is summarized in Table 2. Details of the *FUSE* instrument may be found in Moos et al. (2000) and Sahnou et al. (2000). Note that the LWRS spectra of HD 90087 were first reported in the atlas of Galactic OB *FUSE* spectra presented by Pellerin et al. (2002).

The one-dimensional spectra were extracted from the two-dimensional detector images and calibrated using version 2.4.1 of the CALFUSE pipeline. The data from each channel and segment (SiC1A, SiC2B, LiF1A, LiF2B, etc.) were co-added separately for each of the two apertures, after wavelength shift corrections of the individual calibrated exposures. We did not sum them because the line spread function (LSF) and the distortions in the wavelength scale are different for the LWRS and MDRS apertures, and even between segments for the same aperture. We fit these datasets simultaneously in the analysis reported below.

For the LWRS spectra, we used the 5 available exposures. In the case of MDRS, the individual spectra present flux variations due to the motions of the target in the aperture, whose spread is larger than the size of the aperture.

We did not include the exposures which have too little flux to be useful, which led us to exclude one or two exposures from the sum of some of the segments. Exceptions are the SiC2 segments, for which we used only 20 of the 32 available exposures; the 12 remaining ones present too little flux, or even no flux at all in certain cases (because the target was out of the aperture during the entire exposure). Because of their good photometric quality, we use the LWRS spectra to set the absolute flux level of the MDRS spectra.

The spectral resolution in the final spectra ranges between ~ 13000 and ~ 18500 , depending on detector segment and wavelength. The final LWRS spectra are plotted in Fig. 1. A sample of the SiC1B MDRS spectrum is shown in Fig. 2 with the H I, D I, and O I lines identified. In that figure, the flux has been multiplied by a factor 1.4 in order to match the LWRS one.

2.3. Data analysis

2.3.1. Overview

We measured the column densities N for several species on this line of sight by fitting Voigt profiles to interstellar absorption lines. We used the profile fitting method presented in detail by Hébrard et al. (2002), which is based on the procedure Owens.f, developed by Martin Lemoine and the French *FUSE* Team (Lemoine et al. 2002). We split each spectrum into a series of small sub-spectra centered on absorption lines, and fitted them simultaneously with Voigt profiles using χ^2 minimization (see Fig. 3). Each fit includes typically one hundred or more spectral windows, and around 300 transitions of neutral atoms, ion, and molecules. The different species are assumed to be in six different clouds: the first one includes H I only, the second one D I, O I, N I, Fe II, and P II, the third one C I and its two excited levels C I* and C I**, the fourth one all the rotational levels of H₂, the fifth one HD, and the last one all the rotational levels of CO.

Note that thanks to the redundancy of *FUSE* spectral coverage, a given transition might be observed in one, two, three, or four different segments (see Fig. 1). In addition, as LWRS and MDRS data are available for a given spectral feature, we can have up to eight independent spectra. These different observations allow for some instrumental artifacts to be identified and possibly averaged out.

The laboratory wavelengths and oscillator strengths (f -values) used in the analysis are from Abgrall et al. (1993a, 1993b) and E. Roueff (private communication) for the molecules, and from Morton (2003) for atoms and ions. Morton (1991) was highly used in the past in the literature for similar studies. Following the publication of that atomic data compilation, some important f -value revisions occurred (Beideck et al. 1994; Verner et al. 1994; Tripp et al. 1996; Savage & Sembach 1996; Howk et al. 2000; Sofia et al. 2000), but for the most part, differences between Morton (1991) and the updated atomic tables from Morton (2003) are small. We point out, however, the case of N I transitions, for which some oscillator strength values have been significantly updated in Morton (2003). Such differences (up to a few tens of percent) would have significant effect on the N I column density measurements. Our analysis takes into account the updated f -values compiled by Morton (2003), including those of N I.

Several parameters are free to vary during the fitting procedure, including the column densities of all the species, the radial velocities of the six interstellar clouds assumed in the fit, their temperatures and turbulent velocities, and the shapes of the stellar continua, which are modeled by low order polynomials. *OWENS* produces solutions that are coherent between all the fitted lines, assuming a given cloud has a single radial velocity, temperature and turbulence. Some instrumental parameters are also free to vary, including the flux background, the spectral shifts between the different spectral windows, and the widths of the Gaussian line spread function used to convolve with the Voigt profiles.

The velocity shifts fitted for the spectral windows are plotted in Fig. 4. They allow the inaccuracies of the *FUSE* wavelength calibration to be corrected. Typically, the velocity corrections are consistent within a few km s^{-1} within a given segment. They are not a smooth function of wavelength, and shifts as high as 10 to 20 km s^{-1} might occur over only a few Ångströms in extreme cases (Fig. 5). Larger velocity corrections might occur from one segment to another. The velocity shifts are relative and we did not attempt to measure absolute (e.g. heliocentric or LSR) velocities. We note that the wavelength distortion problem is generally more severe in *FUSE* data obtained in histogram mode. Since most *FUSE* observations employ the time-tag mode, distortion of the wavelength scale is usually not as bad as the examples shown in Fig. 5 (which were recorded in histogram mode).

The widths of the Gaussian line spread function fitted for the spectral windows are shown in Fig. 6. The averages for the apertures LWRS and MDRS are respectively 11.6 ± 1.2 and 11.0 ± 1.4 *FUSE* pixels (full widths at half maximum). We also attempted to fit all spectral windows with a unique LSF width. The best χ^2 was obtained for a 11.4-pixel width. However, significant variations occur from one segment to the other, and as a function

of the wavelength for a given segment. These averaged widths are in agreement with those reported in Hébrard et al. (2002). Note that during the fits, all the spectra were binned to three *FUSE* pixel samples in order to reduce computing time. Considering the width of the LSF, this binning does not degrade the spectral resolution.

When possible, the saturated lines located on the flat part of the curve of growth were excluded from the fit. Indeed, such saturated lines can introduce systematic effects on column density measurement (Hébrard et al. 2002; Hébrard & Moos 2003; Friedman et al. 2005), mainly because the actual widths of the lines, the velocity structure of the sight line, or the line spread function of the instrument are unknown but expected to be complex. A particular difficulty with distant lines of sight such as HD 90087 is the rarity of unsaturated lines for some species, especially D I and O I, which is caused by high column densities. This is significantly different from local sight lines, for which numerous unsaturated lines are available.

Another relevant difference between the long line of sight toward HD 90087 and those of targets located in the Local Bubble is the number of detected absorption lines. The overview of the *FUSE* HD 90087 spectra plotted in Fig. 1 can be compared with the Fig. 1 in Hébrard et al. (2002), which shows the corresponding *FUSE* spectra for a target located 53 pc away. The HD 90087 spectra are particularly crowded. This is due to stellar lines, which are more numerous here than in the case of the targets used to probe the more local interstellar medium (mainly white dwarfs). In the case of HD 90087, however, the high rotational velocity of this star smooths the stellar continuum. An even bigger effect on the absorption line number arises from interstellar lines, as the column densities here are typically tens or hundreds of times larger than those measured in the Local Bubble. In particular, many H_2 lines are detected in the HD 90087 spectra. This makes line blending a critical problem, which can be resolved with simultaneous fits of all the lines together.

Only one interstellar component, at a given radial velocity, was assumed for the sight line for a given species. This assumption is unlikely to be true but it will have no effect on the column densities measured from unsaturated lines (see tests of this assumption in Hébrard et al. 2002). Thus, we report total column densities, integrated along each line of sight.

The simultaneous fit of numerous lines allows the reduction of statistical and systematic errors, especially those errors due to continua placement, LSF uncertainties, line blending, flux and wavelength calibrations, and atomic data uncertainties. The error bars were obtained using the $\Delta\chi^2$ method presented by Hébrard et al. (2002). We also estimated the error bars by varying the assumptions for the fits. This included the LSF (normally free to vary, but tests were made with fixed LSFs), the velocity structure (several species are assumed to be in the same component, but fits with one component per species were performed) and also the aperture (comparing (a) MDRS and LWRS together, (b) only LWRS, and (c) only MDRS).

We discuss below the different species. The measured column densities and error bars are reported in Table 3 and examples of fits are given in Fig. 3. The $\Delta\chi^2$ curves for N I, O I, and D I are plotted in Fig. 7.

2.3.2. Molecular hydrogen (H_2)

All the rotational levels of H_2 were included in a single interstellar component. The fits used a total of about 120 H_2 absorption lines from rotational levels $J = 0$ to $J = 6$ available in one to eight independent segment/aperture configurations. The $J = 0, 1$ H_2 lines present damping wings and the $J = 4, 5, 6$ that we used are unsaturated. This allows accurate column density measurements to be performed for these five levels. Only saturated lines located on the flat part of the curve of growth are available for the $J = 2, 3$ H_2 transitions; this precludes accurate measurements of their column densities.

The excitation diagram corresponding to the derived H_2 column densities is shown in Fig. 8. H_2 is not thermalized for levels $J \geq 2$. The column densities of the levels $J = 0$ and $J = 1$ give the temperature $T = 78$ K, which can be considered as the kinetic temperature of the H_2 molecular gas. A temperature of 78 K would correspond to $b = 0.8$ km s $^{-1}$. Thus, the single-component Doppler parameter $b \simeq 7$ km s $^{-1}$ that we found for this molecular component is not purely thermal but contains additional contributions from the gas turbulent motions and/or additional velocity components. Note that since the $J = 0, 1$ levels are damped and the $J = 4$ to 6 levels are optically thin, the Doppler parameter we derived is mainly characteristic of the $J = 2, 3$ levels. On another hand, since we did not detect any significant velocity shift between the different rotational levels (all are < 1 km s $^{-1}$), this suggests that these levels arise from the same dominant cloud component(s) on average.

2.3.3. Deuterated molecular hydrogen (HD)

The only HD lines detected in the spectra are those corresponding to the level $J = 0$; no HD lines are detected for $J \geq 1$. Our global fits include the seven HD lines used by Lacour et al. (2005), and also four extra ones at 1007.28 Å (see Fig. 3, left-bottom panel), 925.78 Å, 967.53 Å, and 1042.84 Å. The other HD ($J = 0$) lines are blended with strong lines (as $\lambda 1001.89$ Å and $\lambda 1078.81$ Å, which are lost in saturated H_2 lines) and are not detected. Among those eleven HD lines, the five strongest appear to be saturated or nearly so. We then performed extra fits including only the six weakest HD lines, namely $\lambda 1054.29$ Å, $\lambda 959.82$ Å, $\lambda 967.53$ Å, $\lambda 925.78$ Å, $\lambda 1066.27$ Å, and $\lambda 1105.83$ Å (in decreasing order of f -values). Excluding those five saturated lines increased the HD column density estimate by 0.1 dex, from 14.42 to 14.52. We adopt the latter value.

Interestingly, the radial velocity of the HD lines was found to be systematically redshifted by 4 ± 0.5 km s $^{-1}$ with respect to the velocity of the H_2 lines. According to the error bars, the velocity shift is significant; it is mainly constrained by the 13 spectral windows that include close HD and H_2 lines. By comparison, no velocity shifts were detected between the different rotation levels of H_2 (§ 2.3.2), between the different atomic or ionic species (§ 2.3.4), nor between H I and D I (§ 2.3.8). Thus, the shift between H_2 and HD appears to be an actual effect, and not a systematic effect due to an instrumental artifact. In addition, we found a Doppler parameter for the HD lines of $b \simeq 3.5$ km s $^{-1}$, about half the Doppler parameter estimated for H_2 (mainly constrained by $J = 2, 3$). These two results therefore suggest that

HD and H_2 rotational lines do not trace exactly the same gas conditions. Consequently, the HD and H_2 lines were not assumed to be located in the same component during the fits. This might jeopardize the interpretation of the HD/ $2H_2$ ratio computed from the measured column densities of the two species. Note that a similar radial velocity shift (4.6 km s $^{-1}$) was also detected between H_2 and HD on the sight line to PG 0038+199 (Williger et al. 2005). As numerous different H_2 and HD transitions are used in these two analyses, this suggests that HD tabulated wavelengths are unlikely to be the cause of the velocity shifts. A broad study of H_2 and HD radial velocities toward numerous targets is however mandatory to progress on this issue.

2.3.4. Nitrogen (N I)

Numerous unsaturated N I lines are detected in the *FUSE* spectra of HD 90087. The fits include eight of them, namely $\lambda 955.26$ Å, $\lambda 959.49$ Å, $\lambda 951.29$ Å, $\lambda 955.53$ Å, $\lambda 960.20$ Å, $\lambda 1159.82$ Å, $\lambda 1160.94$ Å, and $\lambda 955.44$ Å (in decreasing order of f -values). Some of these lines are detected in several segments and/or through the two available apertures. Thus, the final fits include 18 independent unsaturated N I lines. These lines were fitted simultaneously with all the other ones, assuming that they are in the same cloud as D I, O I, Fe II, and P II. Indeed, these species are supposed to co-exist in neutral regions (Fe I and P I ionization potentials are respectively 7.9 eV and 10.5 eV, i.e. below the hydrogen ionization potential). We checked this hypothesis by performing fits with these five species in five different components, and we did not detect any significant radial velocity shifts between them. The final error bar reported in Table 3 for $N(N I)$ is small due to the numerous unsaturated lines available.

2.3.5. Oxygen (O I)

Many O I lines are available in the *FUSE* bandpass. However, in the range $\log N(O I) \simeq 17 - 18$, most of those lines are saturated, which precludes accurate column density measurement (see § 3 and Friedman et al. 2005). In this column density range, only one unsaturated O I line is available in the *FUSE* bandpass, namely $\lambda 974.07$ Å. This weak line is blended with three H_2 lines, including two lines (levels $J = 2$ and $J = 5$) with equivalent widths larger than the equivalent width of $\lambda 974$ Å. The third one (level $J = 6$) is negligible. The H_2 contributions to this blend can be calculated thanks to the ~ 120 H_2 lines included in the fits, many of which are unblended. Thus, the shapes of the three $\lambda 974$ Å H_2 lines are well-constrained.

$\lambda 974$ Å is detected in the segments SiC1B and SiC2A, through the two available apertures. Our fits include these four different observations of this line, which reduces potential instrumental effects. The fits of $\lambda 974$ Å observed through MDRS on SiC1B and SiC2A are plotted in Fig. 3. The H_2 ($J = 5$) line seems slightly under-fitted, which might be due to a weak unknown feature. However, this extra absorption appears to be weak enough and far enough from $\lambda 974$ Å to have no significant effect on $N(O I)$.

Measuring a column density from only one transition makes the result highly sensitive to possible errors caused by an erroneous f -value or uncontrolled blends from unknown lines. However, up to now, no clues suggest

such problems. No strong inconsistencies were found between $\lambda 974 \text{ \AA}$ and the stronger O I lines available in the *FUSE* bandpass in the case of BD +28°4211 (Hébrard & Moos 2003). Slight disagreements might be difficult to see, however, as $\lambda 974 \text{ \AA}$ is weak on this sight line. We also measured O I in the sight line of HD 195965 from *FUSE* data, using $\lambda 974 \text{ \AA}$ with the same method as those we use for HD 90087 (see Fig. 9). We obtained $\log N(\text{O I}) = 17.77 \pm 0.06$, in agreement with the value obtained by Hoopes et al. (2003) using $\lambda 1356 \text{ \AA}$, $\log N(\text{O I}) = 17.76 \pm 0.06$. Thus, there are apparently no inconsistencies between $\lambda 974 \text{ \AA}$ and $\lambda 1356 \text{ \AA}$ (the studies of oxygen abundance by Meyer et al. (1998), André et al. (2003), or Cartledge et al. (2004) are based on $\lambda 1356 \text{ \AA}$). The two comparisons we present above suggest that $\lambda 974 \text{ \AA}$ presents no strong oscillator strength inconsistencies nor significant uncontrolled blends (see also § 2.3.7).

2.3.6. Deuterium (D I)

As in the case of O I discussed in the previous subsection, only a few unsaturated D I lines are available in this high column density regime. Strong blending (especially for H₂ lines) and saturation prohibit the use of most of the D I lines. The D I lines of $\lambda 920.7 \text{ \AA}$, $\lambda 922.9 \text{ \AA}$, $\lambda 926.0 \text{ \AA}$, and at larger wavelengths in the Lyman series are all saturated, so we did not include them in the fits. $\lambda 917.9 \text{ \AA}$ is not detected because it is located at $\sim -10 \text{ km s}^{-1}$ from a strong H₂ ($J = 1$) line with damping wings, so it cannot be used to constrain $N(\text{D I})$. We could not obtain a good fit to $\lambda 916.9 \text{ \AA}$. This D I line is blended with two strong lines (O I and H₂ ($J = 3$)) but apparently also with some unknown feature(s).

Our fit therefore includes only two D I transitions, namely $\lambda 916.2 \text{ \AA}$ and $\lambda 919.1 \text{ \AA}$. The first one is available only on segment SiC1B, while the second one is available on both SiC1B and SiC2A. As we use simultaneously the data from the MDRS and LWRS apertures, our fits include a total of six D I lines.

A weak H₂ ($J = 5$) line is located $\sim -30 \text{ km s}^{-1}$ from $\lambda 916.2 \text{ \AA}$. It is weak and far enough to have no significant effects. $\lambda 916.2 \text{ \AA}$ is probably the highest detectable D I in the Lyman series. Indeed, in the high column density regime necessary to produce significant absorption for Lyman lines this high, interstellar absorption lines are too numerous and crowded below 916 \AA , and therefore almost no flux is detected there (see Figs. 1 and 2).

The $\lambda 919.1 \text{ \AA}$ D I line is blended with H₂ ($J = 4$), located $\sim 20 \text{ km s}^{-1}$ blueward and of similar equivalent width. The fits include nine other H₂ ($J = 4$) lines, observed on different segments and through the two apertures, allowing the blend to be deconvolved. $\lambda 919.1 \text{ \AA}$ is slightly saturated. We tested the results by including only $\lambda 916.2 \text{ \AA}$, and the ensuing $N(\text{D I})$ was in agreement with the fit to $\lambda 919.1 \text{ \AA}$.

The choice of the continuum used for fitting the absorption lines has an effect on the measured column density. Here the continua are fitted by polynomials for each spectral window. As the parameters of the polynomials are free to vary, the uncertainty due to the continuum should be included in the final error bar. We checked that by varying the continua, i.e. by using different polynomial degrees or

changing the wavelength intervals on which they are fitted.

Our result is $\log N(\text{D I}) = 16.16 \pm 0.12 (2\sigma)$. To date, this is the largest published D I column density ever measured. As $\lambda 916.2 \text{ \AA}$ would saturate for $N(\text{D I})$ values 2 or 3 times larger, it would be difficult to accurately measure larger D I column densities for other sight lines. Note, that this limit also provides a selection bias against sight lines with higher D/H or D/O ratios in this high column density regime. Interesting lower limits on $N(\text{D I})$ might however be estimated from saturated D I lines.

The column density of HD represents only $2.3 \pm 1.0 \%$ (2σ) of $N(\text{D I})$. Most of the deuterium detected on the line of sight of HD 90087 is in atomic form. Therefore, given the size of the errors, deuterium in molecular form can be neglected for the computation of the total deuterium column density.

2.3.7. Other species

(Fe II, P II, Ar I, C I, C I*, C I**, CO)

Interstellar absorption lines of CO, Ar I, Fe II, P II, C I and its two excited levels C I* and C I** are also detected in the spectra of HD 90087. We report accurate column density measurements for CO, Fe II, and P II. The measurements for the remaining species are more uncertain. We discuss here briefly all these species.

Numerous unsaturated Fe II lines are available in the *FUSE* spectra of HD 90087. We used the following ones: $\lambda 1142.4 \text{ \AA}$, $\lambda 1064.0 \text{ \AA}$, $\lambda 1062.2 \text{ \AA}$, $\lambda 1127.1 \text{ \AA}$, and $\lambda 1083.4 \text{ \AA}$ (in decreasing order of f -values). We also made fits including these lines and $\lambda 1055.3 \text{ \AA}$ and $\lambda 1133.7 \text{ \AA}$, whose f -values are larger and which might be slightly saturated. No significant difference was found.

For P II, we used only $\lambda 1124.9 \text{ \AA}$, since $\lambda 1152.8 \text{ \AA}$ is saturated. As Fe II, the P II lines are at the same radial velocity as D I, O I, and N I. Leboutellier et al. (2005) show that P II might be considered as a good proxy for O I. The P II/O I ratio we measure toward HD 90087 is in good agreement with the average ratio they report. This is another argument to support the reliability of our measured $N(\text{O I})$, based on $\lambda 974 \text{ \AA}$ (see § 2.3.5).

The CO A-X bands at 1076 \AA and 1088 \AA were also detected toward HD 90087. Since the band structure cannot be resolved with the *FUSE* data, we included J levels up to $J = 7$ in our initial fits. Our best fit indicated that the column densities of the $J = 0$ and 1 rotational levels are similar while the contribution from the $J \geq 2$ levels is negligible (column densities ten times lower or less). The CO lines are detected at the same radial velocity as H₂. In both regions, there is one $J = 0$ CO transition, and two $J = 1$ CO transitions on each side of the first one. The lines are broad enough to allow the two J -levels to be measured, despite their not being resolved. The excitation diagram leads to a temperature T_{ex} of about 4 K, indicating that the rotational levels are sub-thermally populated. The derived CO/H₂ ratio is $(6.5 \pm 1.4) \times 10^{-7}$ (see Table 4), a value about 3 orders of magnitude smaller than that typically found in purely molecular clouds. The latter results are consistent with rotational population distributions and CO abundances typically found in diffuse molecular clouds where photo-processes still largely dominate the gas chemical pathways (Sonnentrucker et al. 2003).

For carbon, the strongest C I line, at 945 \AA , is near

to saturation. Numerous weaker C I lines are detected in the range 1103 – 1111 Å, together with C I* and C I** transitions. However, it is not possible to obtain a fit in agreement for the different transitions. This is probably due to inaccurate f -values. Using a large sample of interstellar C I lines recorded at high resolution, Jenkins & Tripp (2001) have shown that many C I f -values require significant revisions, especially f -values of weak transitions. Unfortunately, they did not analyze C I transitions in the *FUSE* wavelength range. Our reported carbon column density measurements therefore remain inaccurate.

Finally, $N(\text{Ar I})$ is obtained only from saturated lines ($\lambda 1066.7 \text{ \AA}$ and $\lambda 1048.2 \text{ \AA}$) on the flat part of the curve of growth; it is thus uncertain.

2.3.8. Hydrogen (H I)

To determine the total H I column density in the interstellar medium toward HD 90087, we fitted the damped Ly- α profile recorded in an *IUE* spectrum of the star. HD 90087 was observed with *IUE* once in 1982 (Table 2). We retrieved the IUESIPS (*IUE Spectral Image Processing System*) version of the data and extracted the spectrum using standard procedures. Fig. 10 shows the portion of the spectrum in the vicinity of the Ly- α line. The strongly damped Ly- α profile is readily apparent along with the nearby N V P Cygni profile (which causes the emission feature at $\sim 1241 \text{ \AA}$ and the adjacent trough at $\sim 1239 \text{ \AA}$) and a variety of stellar and interstellar absorption lines.

We measured $N(\text{H I})$ using the procedure described in Jenkins et al. (1999) and Sonneborn et al. (2000). Briefly, we used minimized χ^2 in order to determine the H I column that provided the best fit to the Lorentzian wings of the Ly- α profile. The following five parameters were freely varied using Powell’s method (Press et al. (1995): (1) $N(\text{H I})$, (2)-(4) three coefficients of a low-order polynomial fitted to the continuum over a broad range on each side of Ly- α , and (5) a correction for the flux zero level. HD 90087 is an early-type star, and any stellar Ly- α line is unlikely to significantly affect the interstellar Ly- α profile, especially since the interstellar H I column toward this star turns out to be large and the Ly- α profile is accordingly quite broad. To evaluate upper and lower confidence limits on $N(\text{H I})$ based on changes in χ^2 , we then increased (or decreased) the H I column density while allowing the other parameters to vary. By allowing the polynomial coefficients to vary throughout the entire process, the fitting procedure can adjust the height and curvature of the continuum and thereby provide some assessment of the continuum placement uncertainty. With *IUE* data, background subtraction near Ly- α is difficult due to order crowding, and this introduces significant uncertainty in the flux zero point. For this reason, it is important to include the flux zero point as a free parameter in the fitting process. Our final best fit and the corresponding continuum placement are shown in Fig. 10 along with the profiles corresponding to 1σ upper and lower limits on $N(\text{H I})$. From these fits we obtain $\log N(\text{H I}) = 21.17 \pm 0.10$ (2σ uncertainties).

This result is in good agreement with the values obtained from the fits of Ly- β , Ly- γ , and Ly- δ observed with *FUSE*. We obtained $\log N(\text{H I}) = 21.19 \pm 0.10$ from the fits of these three lines (Fig. 11), using all the available data. However, if Ly- β presents damping wings, the stel-

lar continuum at this wavelength is a critical issue. It is probably reached by strong O VI features due to the stellar wind (see, e.g. Bianchi & Garcia 2002). No robust models of the stellar continuum are available up to now. The polynomials that we used give an estimation of the stellar continua shape, but they are probably too naive. Thus, we adopt the Ly- α measurement for our $N(\text{H I})$ result.

On this line of sight, a minority of the material is in molecular form. The hydrogen molecular fraction $f(\text{H}_2) \equiv 2N(\text{H}_2)/[2N(\text{H}_2) + N(\text{H I})] = 10.1 \pm 2.6 \%$. Thus, molecular species can be neglected when the abundances are computed from column densities ratios. The implied errors on abundance would be of the order of 10 %, probably even less, as the molecular species are unlikely to significantly coexist in the same clouds with the atomic and ionic species. By comparison with the final reported error bars, the effect of the molecules on the abundance is negligible. For example, we obtain $\text{D I}/\text{H I} = (9.8 \pm 3.8) \times 10^{-6}$ and $(\text{D I} + \text{HD})/(\text{H I} + 2\text{H}_2) = (8.9 \pm 3.3) \times 10^{-6}$.

On the contrary to H_2 and HD (§ 2.3.3), we did not detect any significant velocity shifts between the D I and H I lines ($< 1 \text{ km s}^{-1}$) on the *FUSE* spectra, which is reassuring as the ratio of the column densities of these two species are directly used to compute the D/H ratio. Some targets have been reported with significant shifts between the D I and H I lines. Wood et al. (2004), for example, reported a shift of 5 km s^{-1} between the radial velocities of H I and D I on the sight line of JL 9.

2.4. Discussion

The abundances on the line of sight to HD 90087 are reported in Table 4. The D/H, D/O, and D/N ratios are all significantly lower than the ratios measured within the Local Bubble. This is in agreement with the picture reported by Hébrard & Moos (2003), which suggests that the deuterium abundance is significantly lower in the distant interstellar medium than locally.

The N/H ratio is in good agreement with the typical interstellar N/H ratio reported by Meyer et al. (1997). The O/H ratio is rather large when compared with the typical O/H ratios in the distant interstellar medium (Meyer et al. (1998; André et al. 2003; Cartledge et al. 2004), although compatible within the error bars. Other targets have been found to show similar O/H ratios: HD 91824, HD 122879, HD 12323 (Cartledge et al. 2004), HD 195965 (Hoopes et al. 2003), and JL 9 (Wood et al. 2004). It can be argued that the low D/O observed toward HD 90087 is due to the high O/H ratio rather than to a true low deuterium abundance. However, the D/H and D/N ratios are low as well. In addition, if we assume the O I column density is overestimated by a factor ~ 1.6 (in order to agree with the above O/H studies), this would still imply a low D/O, below 3×10^{-2} . The deuterium abundance seems thus to be actually low on this line of sight. It is interesting to note that HD 90087 shows simultaneously a low deuterium abundance together with a rather high oxygen abundance. HD 195965 (Hoopes et al. 2003) and JL 9 (Wood et al. 2004) also show a similar effect. This might be a hint of an astration signature.

The HD/2H $_2$ ratio is about 5 times lower than the D/H ratio. This is characteristic of interstellar clouds with moderate molecular fraction (We obtain $f(\text{H}_2) = 10.1 \pm 2.6 \%$).

Indeed, compared to H_2 , self-shielding of HD becomes significant deeper in the molecular clouds since deuterium is much less abundant than hydrogen (Ferlet et al. 2000; Lacour et al. 2005). Thus, the transition between D I and HD takes place deeper in the molecular clouds than the transition between H I and H_2 . Our HD/ 2H_2 ratio is similar to those reported by Lacour et al. (2005).

3. THE FEIGE 110 LINE OF SIGHT

3.1. *The target*

An extensive study of the Feige 110 sight line was performed by Friedman et al. (2002). All the information about this target and its observations are in that initial paper. Briefly, Feige 110 is a sdOB star. Most of the interstellar material probed along its sight line is probably located outside the Local Bubble. The parallax and photometric distances, 179_{-67}^{+265} pc and 288 ± 43 pc respectively, are in good agreement. Its high Galactic latitude ($-59^\circ 07'$) locates Feige 110 at $z \simeq -150$ pc from the Galactic plane.

The *FUSE* spectra of Feige 110 were obtained in 2000 (Table 2). Friedman et al. (2002) measured $N(\text{D I})$ and $N(\text{O I})$ from these spectra, and used *IUE* archival data to derive $N(\text{H I})$ using the same technique we applied to HD 90087 (§2.3.8). Subsequently, Hébrard & Moos (2003) used the *FUSE* spectra of Feige 110 to measure $N(\text{N I})$ on this sight line.

The O I column density measurement reported by Friedman et al. (2002) was derived using only a curve-of-growth analysis. However, the weak O I line at $\lambda 974.07 \text{ \AA}$ (see § 2.3.5) was not included in this early analysis, and all the O I lines fitted in the curve-of-growth are likely to be significantly saturated. As saturated lines might lead to erroneous column density evaluations (Friedman et al. 2005), we revisit here the $N(\text{O I})$ measurement toward Feige 110.

3.2. *The O I column density revisited*

We used exactly the same dataset previously employed by Friedman et al. (2002) and Hébrard & Moos (2003). As for HD 90087 (§2.3.1), we measured the column densities on the sight line toward Feige 110 using the profile fitting method presented by Hébrard et al. (2002), which is based on the procedure Owens.f (Lemoine et al. 2002). D I, O I, N I, and H_2 lines were included in the fits. We focus here on O I. We note that we obtain results in agreement with Friedman et al. (2002) and Hébrard & Moos (2003) for $N(\text{D I})$ and $N(\text{N I})$, respectively.

As for HD 90087, we found that $\lambda 974.07 \text{ \AA}$ is the only unsaturated O I line available in the *FUSE* bandpass. However, this line is less blended in the case of Feige 110: $\lambda 974.07 \text{ \AA}$ is blended with only one H_2 ($J = 2$) absorption (see Fig. 12). The shape of this saturated H_2 line is constrained thanks to the other H_2 transitions available in the Feige 110 *FUSE* spectra. The two other H_2 transitions located around 974.07 \AA (corresponding to the level $J = 5$ and $J = 6$) are negligible for this sight line. Our fits include the two different available observations of $\lambda 974 \text{ \AA}$ (segments SiC1B and SiC2A).

We checked the results of our fits by performing a curve-of-growth analysis, using the same procedure as Friedman et al. (2002). We normalized the spectrum by a fitted continuum and a synthetic H_2 model constrained by the other

H_2 transitions. Then, as we did for the other, stronger O I lines, we measured the equivalent width of $\lambda 974 \text{ \AA}$. We obtained $13.1 \pm 2.7 \text{ m\AA}$ and $16.8 \pm 2.7 \text{ m\AA}$ for the segments SiC1B and SiC2A, respectively. The resulting curve of growth is plotted in Fig. 13. The column densities measured using these two methods (profile fitting and curve of growth) are different by only 0.03 dex. This difference is negligible with respect to the uncertainties (± 0.15 dex, 2σ), so there are apparently no systematic effects due to the method.

Our final value, which reflects the combined effort of these two independent analyses, is $\log N(\text{O I}) = 17.06 \pm 0.15$. This is a factor ~ 2 larger than the one reported by Friedman et al. (2002), namely $\log N(\text{O I}) = 16.73 \pm 0.10$ (2σ). Fig. 12 shows the fit of $\lambda 974 \text{ \AA}$ using these two $N(\text{O I})$ values, which clearly suggests a higher value than the one reported by Friedman et al. This illustrates that measuring column densities from saturated lines might lead to erroneous results and underestimation of error bars.

Our past experience with different *FUSE* targets together with simulations of *FUSE* data (Moos et al. 2002; Hébrard et al. 2002; Friedman et al. 2005) has shown that measurements from saturated lines seem to preferentially underestimate $N(\text{O I})$. The case of Feige 110 is in agreement with this tendency. We note that the value of $f\lambda$ for $\lambda 974 \text{ \AA}$ is at least 10 times smaller than for the other O I lines in the *FUSE* bandpass. Such large differences might explain significant systematic effects due to saturation in the range $\log N(\text{O I}) \simeq 17 - 18$ when the $\lambda 974 \text{ \AA}$ transition is not used in the analysis. In addition, one can note that the equivalent width of the $\lambda 919.917 \text{ \AA}$ O I line seems to indicate a lower column density (see Fig. 13). The reason is unclear, but it can be due to structure along the sight line, some components being saturated before the other ones. A slight inaccuracy in f -value for the $\lambda 919.917 \text{ \AA}$ transition and/or blending issue implying continuum uncertainties in that spectral area might also be present. Such problems with $\lambda 919.917 \text{ \AA}$ might increase the error for $N(\text{O I})$ even more, if $\lambda 974 \text{ \AA}$ is not used.

Targets in that column density range ($\log N(\text{O I}) \simeq 17 - 18$) and with poor signal to noise should be considered with caution. Indeed, if the signal to noise is not high enough to allow $\lambda 974 \text{ \AA}$ to be detected, $N(\text{O I})$ measurements might be significantly underestimated (see the dashed line in Fig. 13).

Since it is mainly based on one transition, our final result on $N(\text{O I})$ toward Feige 110 is highly sensitive to possible errors caused by uncontrolled blends from unknown lines (numerous stellar lines due to metals are detected in the spectrum of Feige 110) or an erroneous f -value. Up to now, studies of other targets have not suggested such problems (see § 2.3.5 and Friedman et al. 2005).

3.3. *Discussion*

Using our new O I column density measurement together with the $N(\text{D I})$ reported by Friedman et al. (2002), we obtain $\text{D/O} = (2.6 \pm 1.0) \times 10^{-2}$ (2σ). This ratio is lower than D/O measured in the Local Bubble, $(\text{D/O})_{\text{LB}} = (3.84 \pm 0.16) \times 10^{-2}$ (1σ , Hébrard & Moos 2003). The lower D/O value is in agreement with the fact that the deuterium abundance might be lower for the most distant

lines of sight and the highest column densities, as reported by Hébrard & Moos (2003).

Friedman et al. (2002), however, reported $D/H = (2.14 \pm 0.82) \times 10^{-5}$ (2σ) on this sight line. This ratio is *larger* than the Local Bubble value, which is in the range $(1.3 - 1.5) \times 10^{-5}$ (see § 1). This ratio is also about three times larger than the D/H typical from the distant interstellar medium reported by Hébrard & Moos (2003). The apparent contradiction between D/H and D/O is surprising. Thus, this sight line appears atypical.

According to our new evaluation of $N(O\ I)$ and the $N(H\ I)$ from Friedman et al. (2002), the oxygen abundance toward Feige 110 is $O/H = (8.3 \pm 4.6) \times 10^{-4}$ (2σ). This ratio is about two times larger than the typical O/H ratios reported by Meyer et al. (1998), André et al. (2003), or Cartledge et al. (2004).

Similarly, the $N(N\ I)$ measurement from Hébrard & Moos (2003) and the $N(H\ I)$ measurement from Friedman et al. (2002) imply $N/H = (2.4 \pm 1.5) \times 10^{-4}$ (2σ) for Feige 110. This ratio is about three times larger than the typical N/H ratios reported by Meyer et al. (1997).

The fact that D/H , O/H , N/H are all approximately two-three times larger than the values usually measured in the distant interstellar medium is suspicious. It suggests that the $H\ I$ column density might be affected by some systematic effects, and the actual $N(H\ I)$ being two-three times larger. However, the IUE $Ly-\alpha$ spectrum of Feige 110 studied by Friedman et al. (2002) appears not consistent with such a high $H\ I$ column density. New $Ly-\alpha$ observations would be very useful for that target but due to the recent failure of the spectrograph STIS onboard HST, such observations won't be possible at short term. Whatever the solution is, Feige 110 appears as an abnormal line of sight, with abnormally high D/H , O/H , and N/H ratios.

Finally, the Ti/H ratio appears also particularly high toward Feige 110 (Prochaska et al. 2005). This point is important, as Feige 110 is the target that mainly drives the correlation between $D\ I$ and $Ti\ II$ recently reported by Prochaska et al. (2005). Such a correlation might be interpreted as a support for a significant depletion of deuterium onto dust grains (Linsky et al. 2005), as Ti is a refractory element. However, the systematic effect that we suspect on $N(H\ I)$ might also be the cause for the high Ti/H ratio measured toward Feige 110.

4. COMPARISON OF D/H AND D/O MEASUREMENTS

In this section we compare our new D/H and D/O measurements with those obtained toward other lines of sight. D/O is considered to be a good proxy for D/H and, in addition, it may be less sensitive to systematic effects (Timmes et al. 1997; Hébrard & Moos 2003).

Fig. 14 (left panel) shows D/O as a function of the $D\ I$ column density. This plot includes 27 sight lines: the 24 included in Hébrard & Moos (2003), but with the revised $N(O\ I)$ for Feige 110 (§ 3), plus JL 9 (Wood et al. 2004), PG 0038+199 (Williger et al. 2005), and HD 90087 (§ 2). Thus, D/O measurements apparently show a bimodal picture: there is a high, homogeneous D/O ratio for low $D\ I$ column densities, and a low, homogeneous D/O ratio for high $D\ I$ column densities. The weighted mean for the 14 lines of sight within the Lo-

cal Bubble is $(D/O)_{LB} = (3.84 \pm 0.16) \times 10^{-2}$ (Hébrard & Moos 2003). The weighted mean for the 7 lines of sight with the highest $N(D\ I)$ is about two times lower: $D/O = (1.75 \pm 0.18) \times 10^{-2}$, with a χ^2 of 5.9 for 6 degrees of freedom (reduced χ^2 of 1.0). We do not see any variations in the distant D/O ratio. These 7 sight lines are Feige 110 (Friedman et al. 2002 and § 3), HD 195965 and HD 191877 (Hoopes et al. 2003), LSS 1274 (Hébrard & Moos 2003; Wood et al. 2004), JL 9 (Wood et al. 2004), PG 0038+199 (Williger et al. 2005), and HD 90087 (§ 2); they all present $\log N(D\ I) > 15.4$. The transition between the two D/O ratios, 3.84×10^{-2} and 1.75×10^{-2} , is located around $\log N(D\ I) \simeq 15 - 15.3$.

This simple, bimodal picture of D/O is rather different from what D/H shows. Indeed, a larger dispersion is seen through D/H measurements. On Fig. 14 (right panel) are plotted D/H ratios as a function of $\log N(D\ I)$ for 43 lines of sight. This includes the 39 targets reported in the Table 4 from Wood et al. (2004), to which we added Sirius (Hébrard et al. 1999), Lan 23 (Oliveira et al. 2003), PG 0038+199 (Williger et al. 2005), and HD 90087 (§ 2). Note that we adopt $D/H = (2.2^{+0.4}_{-1.2}) \times 10^{-5}$ for Lan 23, according the $D\ I$ and $H\ I$ column densities reported by Oliveira et al. (2003). The $N(H\ I)$ toward this target is derived from low EUVE flux, which makes the measurement uncertain, especially for such high column density. The x -axes of the two plots of Fig. 14 are identical, and their y -axes are scaled to the same size (assuming $O/H = 3.43 \times 10^{-4}$; Meyer 2001); this allows the two panels to be easily compared.

Within the Local Bubble, at low $D\ I$ column densities, both panels show a homogeneous deuterium abundance (note the slight but significant disagreement between the two averaged values; see Hébrard & Moos 2003). However, the two panels present different pictures at larger column densities: whereas D/O shows a decrease toward a homogeneous value, D/H shows dispersions. Considering as above the same 7 lines of sight with $\log N(D\ I) > 15.4$, the χ^2 for the weighted mean of this D/H distribution is 34.4, whereas it is 5.9 in the case of D/O (for 6 degrees of freedom in both cases). D/H seems more dispersed than D/O in the distant interstellar medium.

Since oxygen is considered as a good proxy for hydrogen, these two different pictures are unexpected. This discrepancy might call into question the homogeneity of the O/H ratio within the interstellar medium, but numerous studies show that $O\ I$ is a good tracer of $H\ I$ in the nearby Galactic disk (Meyer et al. 1998; André et al. 2003; Cartledge et al. 2004; Oliveira et al. 2005). André et al. (2003) and Cartledge et al. (2004) suggested however O/H can vary somewhat as a function of distance and/or average density. On another hand, it can be argued that some $H\ I$ column densities are under-evaluated, as it may be possible for Feige 110 (§ 3), but no systematics allowing such under-evaluation have been yet clearly identified. Fig. 13 in Williger et al. (2005) shows explicitly how poor the PG 0038+199 $Ly-\beta$ line is fitted if $N(H\ I)$ is forced to be high enough to recover the expected D/H and O/H values. $O\ I$ column densities might also be suspected to be erroneous for distant lines of sight, as it is mainly measured from only one transition, namely $\lambda 974.07\ \text{\AA}$. This transition appears however to be reliable

(§ 2.3.5), and there are several targets that show low D/O ratios whereas their $N(\text{O I})$ measurements are based on $\lambda 1356 \text{ \AA}$ (δ Ori A, γ Cas, ϵ Ori, HD 195965; see Hébrard & Moos 2003). Finally, if deuterium is significantly depleted onto dust grains, as proposed by Wood et al. (2004) and Linsky et al. (2005), one would have to argue that oxygen is depleted at the same rate, in order explain the observed constancy of D/O and variability of D/H. Such a tight correlation between deuterium and oxygen depletion seems unlikely, however. Indeed, oxygen tends to be associated with silicates, whereas Draine (2004) proposed that PAHs are causing the deuterium depletion. Up to now, the discrepancy between the constancy of D/O and the variability of D/H remains unexplained. Several processes might be implied, including the above ones, but the complete explanation is still to be found.

It should also be recalled that distant targets with deuterium measurements remain sparse. Actually, only three lines of sight exhibit significantly high D/H ratios, namely PG 0038+199, Feige 110, and γ^2 Vel. These targets are important as they are those that are assumed to be characteristic of the actual $(\text{D}/\text{H})_{\text{PE}}$ value if deuterium is significantly depleted onto dust grains. For the two first ones, both D/H and D/O measurements are available. For PG 0038+199, $\text{D}/\text{H} = (2.19^{+0.30}_{-0.27}) \times 10^{-5}$ and $\text{D}/\text{O} = (2.40^{+1.03}_{-0.45}) \times 10^{-2}$ (Williger et al. 2005), and for Feige 110, $\text{D}/\text{H} = (2.14 \pm 0.41) \times 10^{-5}$ (Friedman et al. 2002) and $\text{D}/\text{O} = (2.6 \pm 0.5) \times 10^{-2}$ (§ 3). Thus, both present “low” D/O ratios, but “high” D/H. No direct $\log N(\text{O I})$ measurements are available for the last target, γ^2 Vel, for which Sonneborn et al. (2000) reported $\text{D}/\text{H} = (2.18^{+0.22}_{-0.19}) \times 10^{-5}$. The only available estimation is reported by Knauth et al. (2003): $N(\text{O I}) = (5.23 \pm 1.27) \times 10^{16} \text{ cm}^{-2}$. This is based on O I and S II observations by Fitzpatrick & Spitzer (1994). It leads to a low D/O ratio ($\sim 2.1 \times 10^{-2}$), but the systematic uncertainties in this $N(\text{O I})$ indirect estimation are too large to allow any firm conclusion to be drawn. Indeed, using updated solar abundances and a lower depletion factor might produce D/O up to ~ 3.5 times larger.

More D/H and D/O measurements toward distant lines of sight are mandatory to compare the enigmatic behavior of these ratios.

5. CONCLUSION

We have presented a new interstellar deuterium abundance study of the sight line toward HD 90087, and the revision of a result for Feige 110, both based on *FUSE* spectra.

Our new measurement of $N(\text{O I})$ toward Feige 110 shows that O I column density measurements based on saturated lines might be erroneous, even up to a factor of two, and that the error bars might be underestimated due to systematic effects. This sight line exhibits a low D/O ratio, in agreement with those obtained toward other distant targets.

HD 90087 is the farthest Galactic target for which the deuterium abundance has been measured from ultraviolet absorption lines so far, both in terms of distance and column densities. The low deuterium abundance measured on this line of sight is in agreement with the trend reported by Hébrard & Moos (2003) and reinforced by Wood et al. (2004): on large scales, the deuterium abundance is lower than the one measured within the Local Bubble. The question however remains open to know if this low deuterium abundance is the value representative of the present epoch, or the signature that a significant amount of deuterium has been depleted onto dust grains.

Finally, we have shown that D/H presents more dispersion than D/O does. As oxygen is considered to be a good proxy for hydrogen, this discrepancy is puzzling. This might call into question the homogeneity of the O/H ratio, or some H I or O I column density measurements. The complete explanation is still to be found.

This work is based on data obtained by the NASA-CNES-CSA *FUSE* mission operated by the Johns Hopkins University. Financial support has been provided by NASA contract NAS5-32985. We thank D. Massa and A. W. Fullerton for their help on the stellar profile of HD 90087, as well as C. M. Oliveira and A. Vidal-Madjar for useful comments on this paper. Most of this work was performed during the stay of G. H. at the Johns Hopkins University in 2004. G. H. was also supported by CNES. T. M. T. was supported in part by NASA grant NNG 04GG73G. This work used the profile fitting procedure Owens.f developed by M. Lemoine and the French *FUSE* Team.

REFERENCES

- Abgrall, H., Roueff, E., Launay, F., Roncin, J. Y., & Subtil, J. L. 1993, *A&AS*, 101, 323
 Abgrall, H., Roueff, E., Launay, F., Roncin, J. Y., & Subtil, J. L. 1993, *A&AS*, 101, 273
 André, M. K., Oliveira, C. M., Howk, J. C., et al. 2003, *ApJ*, 591, 1000
 Beideck, D. J., Schectman, R. M., Federman, S. R., & Ellis, D. G. 1994, *ApJ*, 428, 393
 Bianchi, L., & Garcia, M. 2002, *ApJ*, 581, 610
 Bowen, D. V., Jenkins, E. B., Tripp, T. M., Sembach, K. R., & Savage, B. D. 2004, in “Astrophysics in the Far Ultraviolet: Five Years of Discovery with FUSE”, eds. G. Sonneborn, H. W. Moos, & B.-G. Andersson (San Francisco: ASP), in press (astro-ph/0410008)
 Cartledge, S. I. B., Lauroesch, J. T., Meyer, D. M., & Sofia, U. J. 2004, *ApJ*, 613, 1037
 Diplas, A. & Savage, B. D. 1994, *ApJS*, 93, 211
 Draine, B. T. 2004, in *Origin and Evolution of the Elements*, ed. A. McWilliams & M. Rauch (Cambridge: Cambridge Univ. Press), p. 320
 Ferlet, R., et al. 2000, *ApJ*, 538, L69
 Fitzpatrick, E.L., & Spitzer, L., Jr. 1994, *ApJ*, 427, 232
 Friedman, S. D. et al. 2002, *ApJS*, 140, 37
 Friedman, S. D. et al. 2005, *ApJ*, submitted
 Hébrard, G., Mallouris, C., Ferlet, R., Koester, D., Lemoine, M., Vidal-Madjar, A., & York, D. 1999, *A&A*, 350, 643
 Hébrard, G. et al. 2002, *ApJS*, 140, 103
 Hébrard, G. & Moos, H. W. 2003, *ApJ*, 599, 297
 Hog, E., Kuzmin, A., Bastian, U., Fabricius, C., Kuimov, K., Lindegren, L., Makarov, V. V., & Roeser, S. 1998, *A&A*, 335, L65
 Hoopes, C. G., Sembach, K. R., Hébrard, G., Moos, H. W., & Knauth, D.C. 2003, *ApJ*, 586, 1094
 Howk, J. C., Sembach, K. R., Roth, K. C., & Kruk, J. W. 2000, *ApJ*, 544, 867
 Jenkins, E. B., Tripp, T. M., Woźniak, P. A., Sofia, U. J., & Sonneborn, G. 1999, *ApJ*, 520, 182
 Jenkins, E. B., & Tripp, T. M. 2001, *ApJS*, 137, 297
 Jura, M. A. 1982, in *Advances in Ultraviolet Astronomy*, ed. Y. Knauth, D. C., Andersson, B.-G., McCandliss, S. R., & Moos, H. W. 2003, *ApJ*, 596, L51

- Lacour, S., André, M. K., Sonnentrucker, P., Le Petit, F., Désert, J.-M., Ferlet, R., Roueff, E., Welty, D. E., York, D. G. 2005, *A&A*, 430, 967
- Laurent, C., Vidal-Madjar, A., & York, D. G. 1979, *ApJ*, 229, 923
- Lebouteiller, V., Kuassivi, & Ferlet, R. 2005, *A&A*, in press (astro-ph/0507404)
- Lemoine, M. et al. 1999, *New Astronomy*, 4, 231
- Lemoine, M. et al. 2002, *ApJS*, 140, 67
- Linsky, J. L. et al. 2005, submitted to *ApJ*
- Mathys, G. 1988, *A&AS*, 76, 427
- Meyer, D. M., Cardelli, J. A., & Sofia, U. J. 1997, *ApJ*, 490, L103
- Meyer, D. M., Jura, M., & Cardelli, J. A. 1998, *ApJ*, 493, 222
- Meyer, D. M. 2001, XVIIth IAP Colloquium, Paris, Edited by R. Ferlet et al., p. 135
- Moos, H. W. et al. 2000, *ApJ*, 538, L1
- Moos, H. W. et al. 2002, *ApJS*, 140, 3
- Morton, D. C. 1991, *ApJS*, 77, 119
- Morton, D. C. 2003, *ApJS*, 149, 205
- Oliveira, C. M., Hébrard, G., Howk, J. C., Kruk, J. W., Chayer, P., Moos, H. W. 2003, *ApJ*, 587, 235
- Oliveira, C. M., Dupuis, J., Chayer, P., Moos, H. M. 2005a, *ApJ*, 625, 232
- Pellerin, A., et al. 2002, *ApJS*, 143, 159
- Press, W., Teukolsky, S., Vetterling, W., and Flannery, B. 1995. *Numerical Recipes in C*. Cambridge University Press, second edition
- Prochaska, J. X., Tripp, T. M., & Howk, J. C. 2005, *ApJ*, 620, L39
- Sahnow, D. J. et al. 2000, *ApJ*, 538, L7
- Savage, B. D., & Sembach, K. R. 1996, *ARA&A*, 34, 279
- Savage, B. D., Meade, M. R., & Sembach, K. R. 2001, *ApJS*, 136, 631
- Sfeir, D. M., Lallement, R., Crifo, F., & Welsh, B. Y. 1999, *A&A*, 346, 785
- Sofia, U. J., Fabian, D., & Howk, J. C. 2000, *ApJ*, 531, 384
- Sonneborn, G., Tripp, T. M., Ferlet, R., Jenkins, E. B., Sofia, U. J., Vidal-Madjar, A., & Woźniak, P. R. 2000, *ApJ*, 545, 277
- Sonnentrucker, P., Friedman, S. D., Welty, D. E., York, D. G., & Snow, T. P. 2003, *ApJ*, 596, 350
- Timmes, F. X., Truran, J. W., Lauroesch, J. T., & York, D. G. 1997, *ApJ*, 476, 464
- Tripp, T. M., Lu, L., & Savage, B. D. 1996, *ApJS*, 102, 239
- Verner, D. A., Barthel, P. D., & Tytler, D. 1994, *A&AS*, 108, 287
- Welsh, B. Y., Sasseeen, T., Craig, N., Jelinsky, S., & Albert, C. E. 1997, *ApJS*, 112, 507
- Williger, G. M., Oliveira, C., ébrard, G., Dupuis, J., Dreizler, S., Moos 2005, *ApJ*, 625, 210
- Wood, B. E., Linsky, J. L., Hébrard, G., Williger, G. M., Moos, H. W., Blair, W. P. 2004, *ApJ*, 609, 838

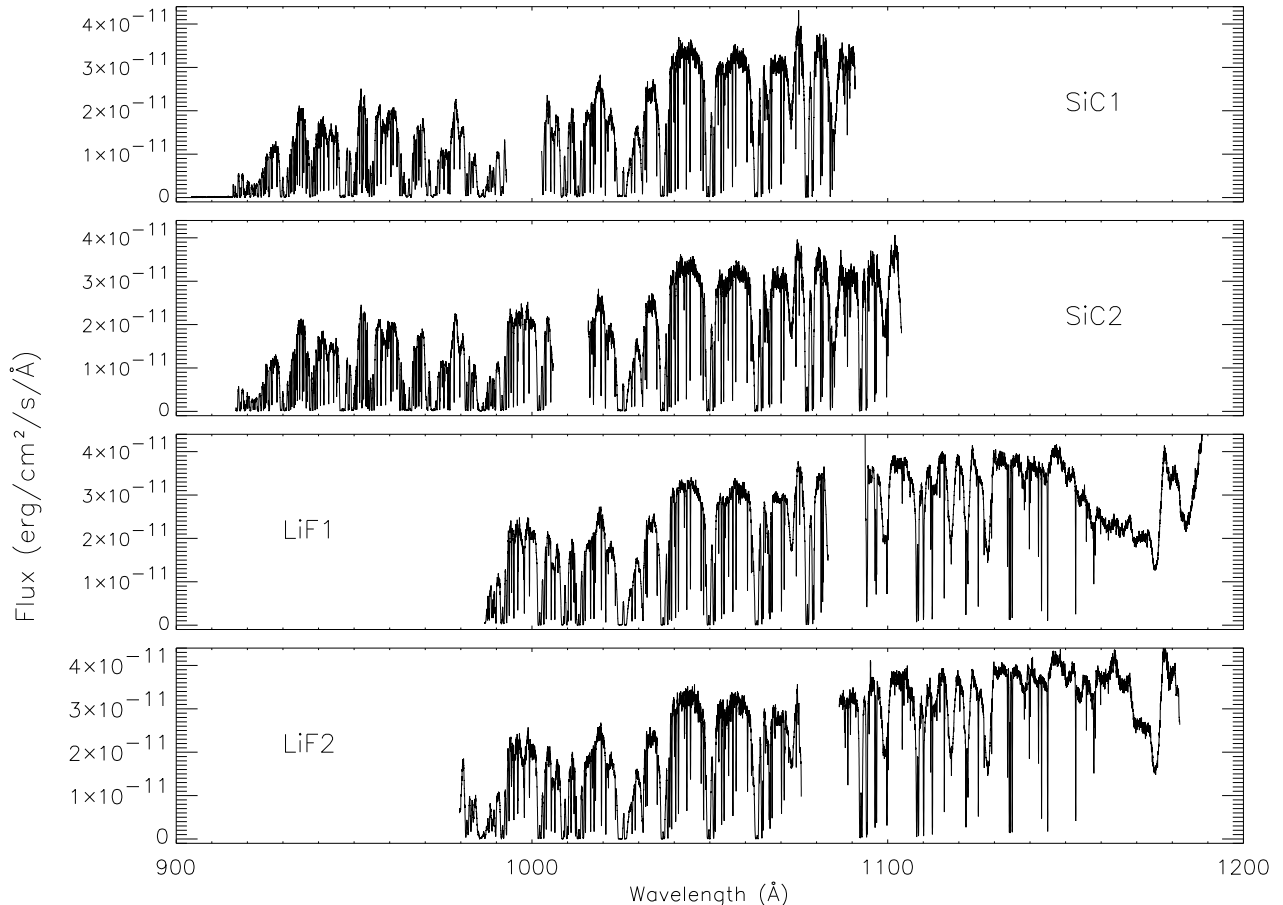


FIG. 1.— The eight segments of the *FUSE* HD 90087 spectra obtained through the large aperture (LWRS). Each channel (SiC1, SiC2, LiF1, and LiF2) is divided in two segments (A and B), separated by a gap. Due to the shorter exposure time, the signal-to-noise ratio is lower for this spectrum than for the spectra obtained through the medium aperture (MDRS), on which most of the analysis is based. The flux calibration is however expected to be better for the LWRS spectra.

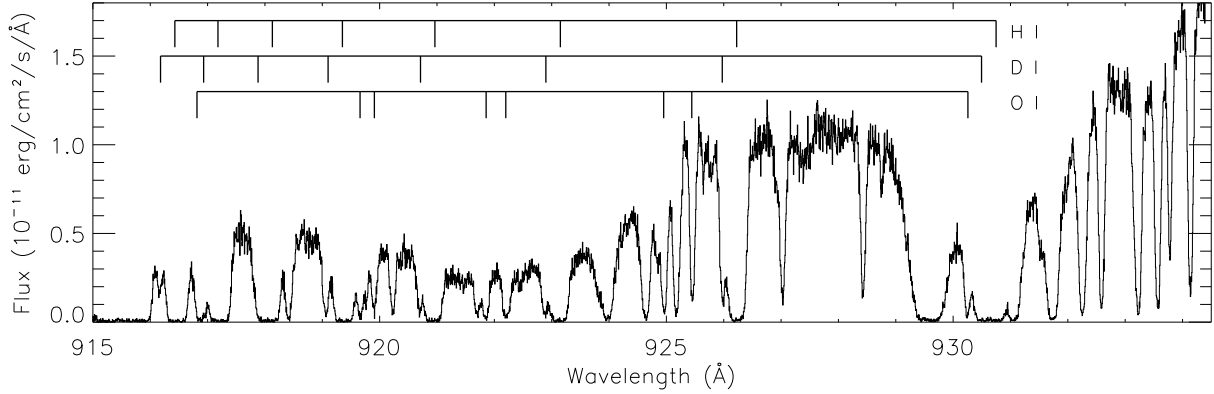


FIG. 2.— Sample of the *FUSE* SiC1B spectrum of HD 90087 observed through the MDRS aperture. Numerous interstellar lines are detected in absorption on the stellar continuum. Positions of H I, D I, and O I interstellar lines are indicated. Most of the remaining absorption lines are H₂ transitions for different *J*-levels.

TABLE 1
HD 90087 SUMMARY.

| Quantity | Value | Reference |
|---|------------------------|-----------|
| Spectral Type | O9.5 III | 1 |
| Right ascension (2000) | 10:22:20.8 | 2 |
| Declination (2000) | −59:45:19.7 | 2 |
| Galactic longitude (<i>l</i>) | 285.15° | 2 |
| Galactic latitude (<i>b</i>) | −2.13° | 2 |
| Distance (<i>d</i>) | 2740 pc | 3 |
| Distance to Galactic plane (<i>z</i>) | −102 pc | 3 |
| Magnitude (<i>V</i>) | 7.80 | 3 |
| <i>E</i> (<i>B</i> − <i>V</i>) | 0.28 | 3 |
| Rotational velocity (<i>v</i> sin <i>i</i>) | 272 km s ^{−1} | 3 |
| Radial velocity (<i>V</i> _{rad}) | −2 km s ^{−1} | 3 |

References – (1) Mathys 1988; (2) Hog et al. 1998; (3) Savage, Meade, & Sembach 2001.

TABLE 2
LOG OF THE OBSERVATIONS.

| Target | Instrument | Obs. date | data ID | <i>T</i> _{obs} ^a | <i>N</i> _{exp} ^b | Apert. ^c |
|-----------|-------------|-------------|----------|--------------------------------------|--------------------------------------|---------------------|
| HD 90087 | <i>FUSE</i> | 2000 Apr 03 | P1022901 | 3.9 | 5 | LWRS |
| HD 90087 | <i>FUSE</i> | 2003 Jun 17 | P3030401 | 14.0 | 32 | MDRS |
| HD 90087 | <i>IUE</i> | 1982 Mar 14 | SWP16532 | 3.9 | 1 | LARGE |
| Feige 110 | <i>FUSE</i> | 2000 Jun 22 | M1080801 | 6.2 | 8 | LWRS |
| Feige 110 | <i>FUSE</i> | 2000 Jun 30 | P1044301 | 21.8 | 48 | LWRS |

^a Total exposure time of the observation (in 10³ s).

^b Number of individual exposures during the observation.

^c LWRS and MDRS are, respectively, large and medium *FUSE* apertures.

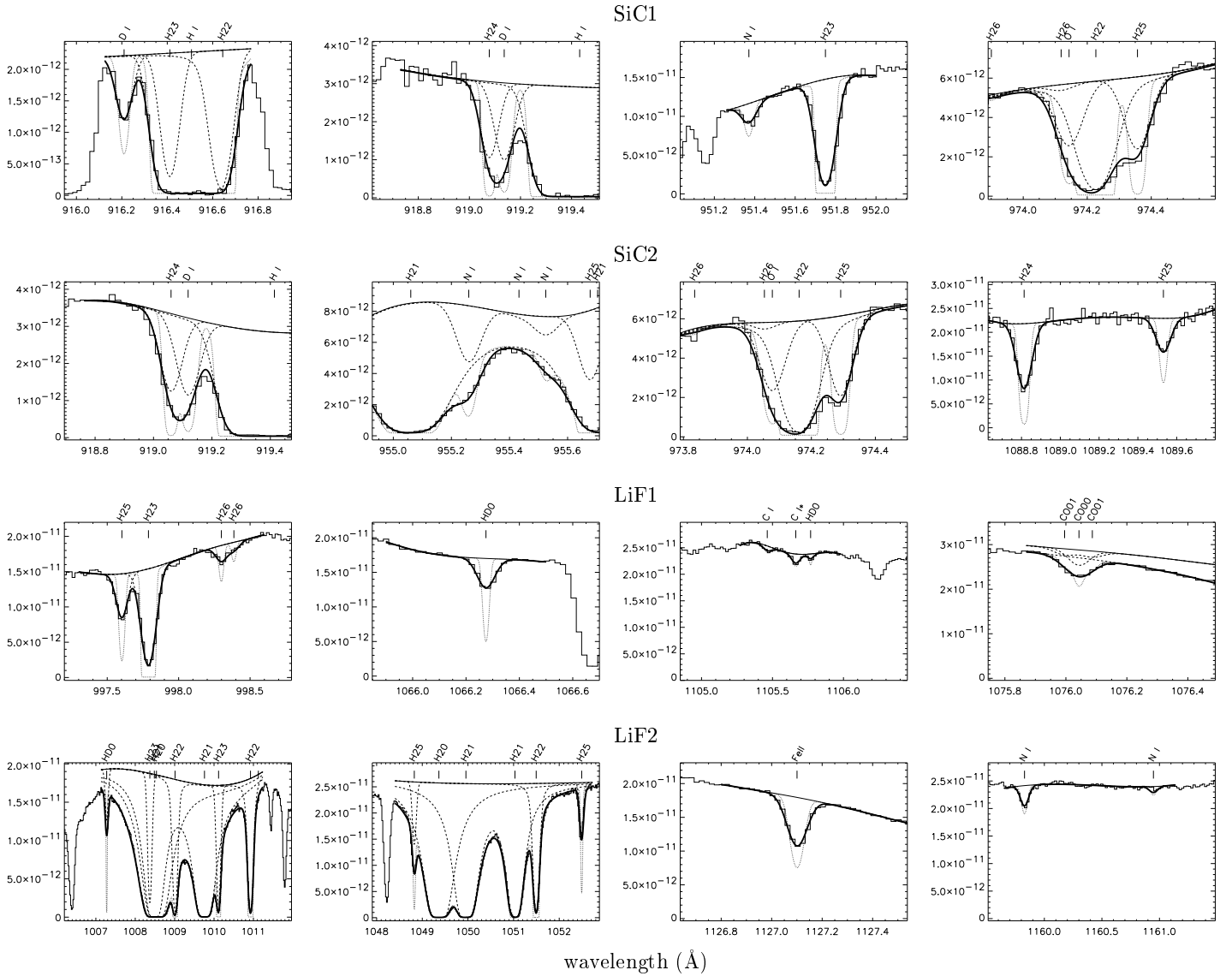


FIG. 3.— Examples of *FUSE* spectral windows fitted on the line of sight of HD90087. Histogram lines are the data, the solid lines are the fits (thick) and continua (thin). The dashed lines are the fits for each species. The dotted lines are the model profiles prior to convolution with the line spread function. The Y-axis is flux in $\text{erg}/\text{cm}^2/\text{s}/\text{\AA}$. The species are identified at the top of the plots for each line. The H_2 lines of the levels $J = 0$ to $J = 6$ are noted H20 to H26, HD ($J = 0$) is noted HD0, and CO $J = 0, 1$ are noted CO00, CO01. We show here only 16 fitting windows for MDRS spectra, including 59 transitions. The complete fits include typically one hundred or more spectral windows on MDRS and LWRs spectra, and around 300 transitions.

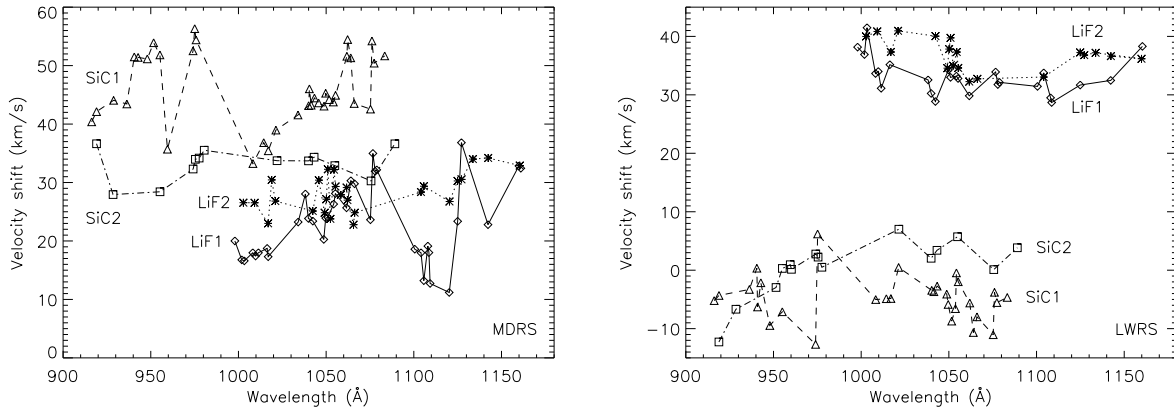


FIG. 4.— Relative velocity shifts fitted for spectral windows on HD 90087 *FUSE* spectra from MDRS (left) and LWRS (right) apertures.

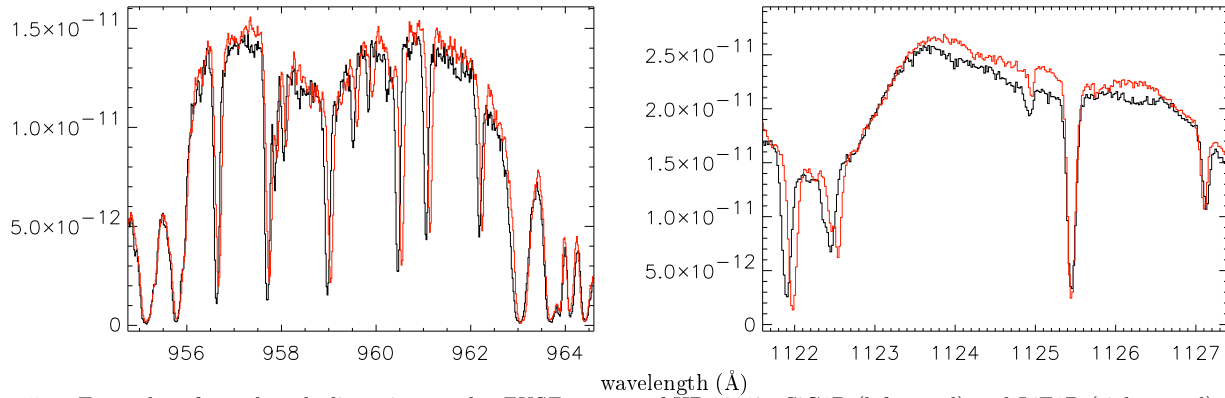


FIG. 5.— Examples of wavelength distortion on the *FUSE* spectra of HD 90087. SiC1B (left panel) and LiF1B (right panel) are in black, and SiC2A (left panel) and LiF2A (right panel) are in red. The Y-axis is flux in $\text{erg}/\text{cm}^2/\text{s}/\text{\AA}$.

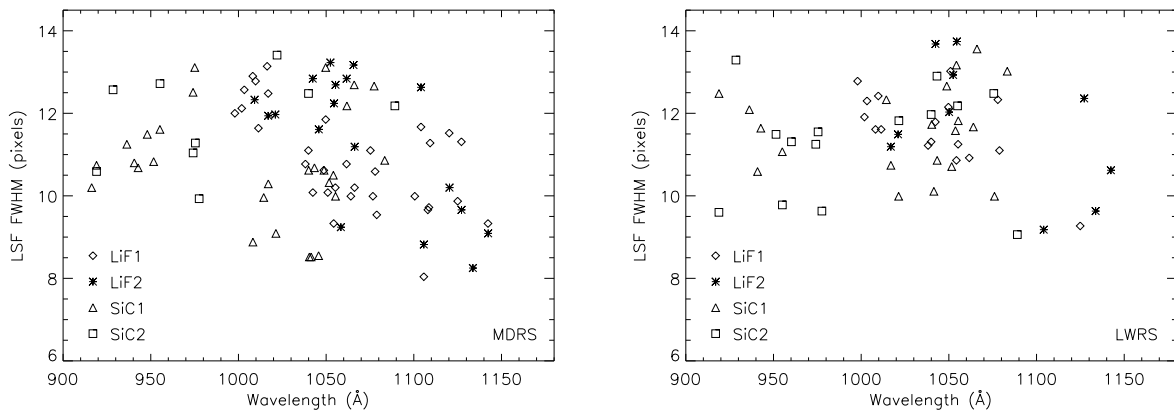


FIG. 6.— Full widths at half maximum (FWHM) of the Gaussian line spread function (LSF) fitted for spectral windows on HD 90087 *FUSE* spectra from MDRS (left) and LWRS (right) apertures.

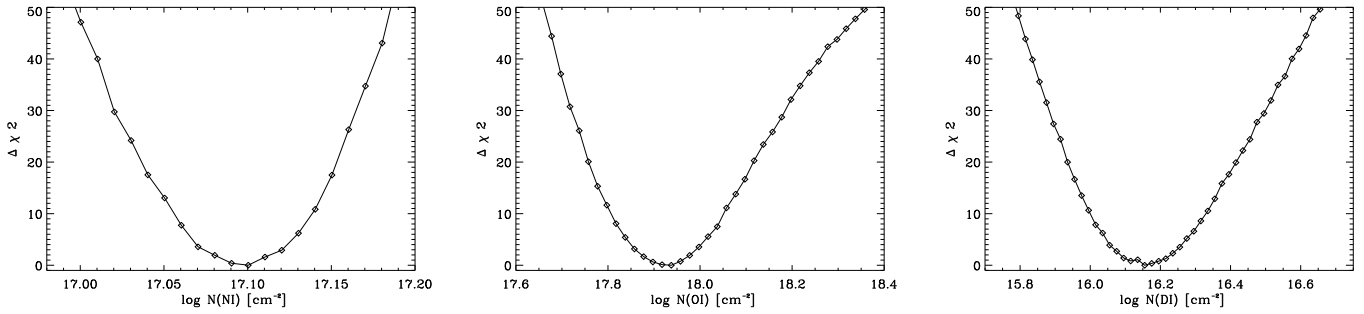


FIG. 7.— $\Delta\chi^2$ curves for N I, O I, and D I toward HD 90087. Each point on these curves corresponds to an individual fit, made with all the parameters free, but the N I, O I, or D I column density fixed. χ^2 values are rescaled on these plots (see Hébrard et al. 2002).

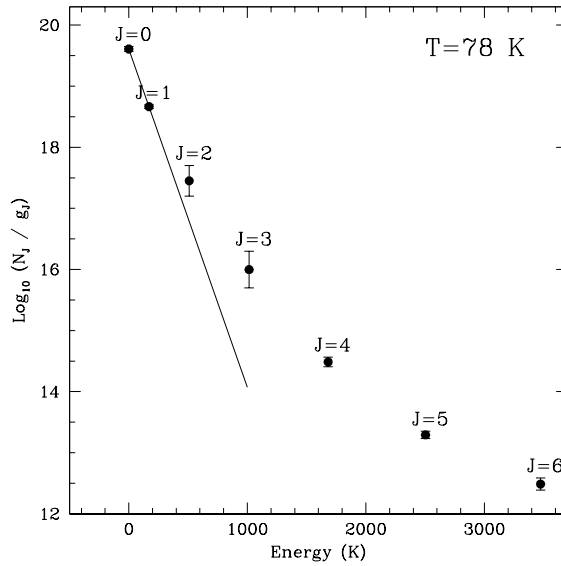


FIG. 8.— Excitation diagram of the H₂ lines detected toward HD 90087. The column densities of the rotational levels $J = 0$ and $J = 1$ are consistent with a temperature $T = 78$ K.

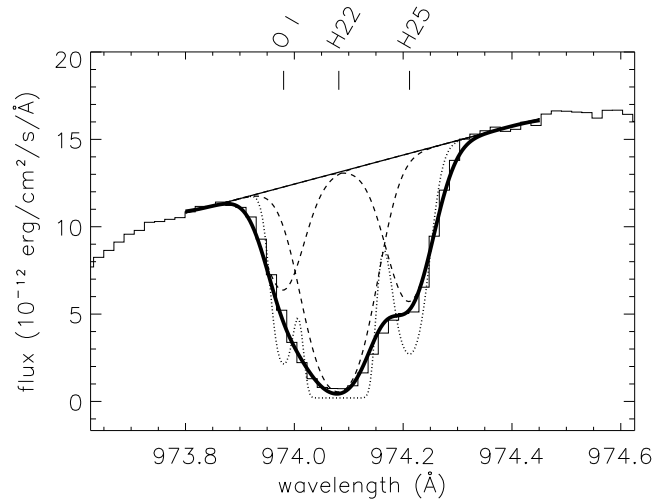


FIG. 9.— Fit of the $\lambda 974.07$ Å O I line as observed for *FUSE* spectra of HD 195965. Same conventions as in Fig. 3. The value $N(\text{O I}) = 17.77 \pm 0.06$ obtained from this fit is in good agreement with those obtained by Hoopes et al. (2003) using the O I line at 1355.60 Å, namely 17.76 ± 0.06 . Apparently, $\lambda 974$ Å presents no strong oscillator strength inconsistencies nor significant unresolved blends.

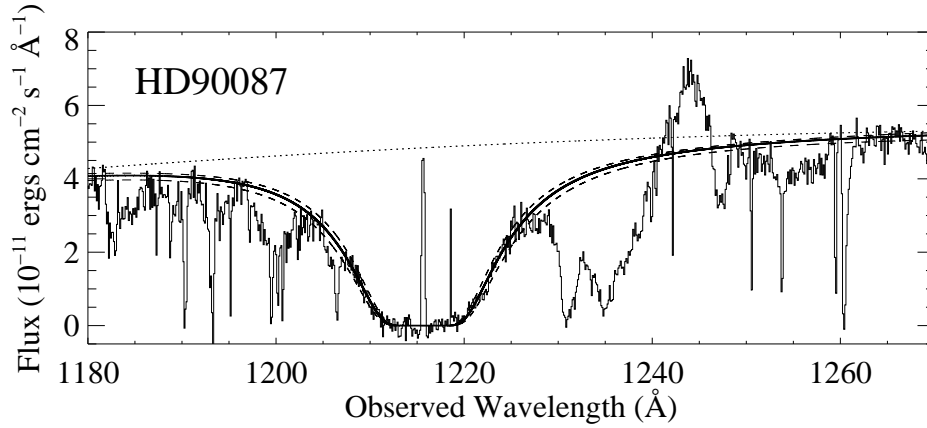


FIG. 10.— Fit of the Ly- α H I line toward HD 90087. The black line is the high resolution *IUE* spectrum. The strongly damped Ly- α profile is readily apparent along with the nearby N V P Cyg profile (λ 1240 Å) and a variety of stellar and interstellar absorption lines. The emission line in the center of the Ly- α profile is the geocoronal H I emission due to the terrestrial atmosphere (the narrow spike at the right edge of the saturated core is a spurious pixel). The solid line shows the best fit, and the two dashed lines show the $\pm 1\sigma$ fits. The dotted line in the plot shows the adopted continuum for the best fit.

TABLE 3

TOTAL INTERSTELLAR COLUMN DENSITIES TOWARD HD 90087.

| species | $\log N(\text{cm}^{-2})^a$ | species | $\log N(\text{cm}^{-2})^a$ |
|----------------------------|----------------------------|------------|----------------------------|
| H ₂ ($J = 0$) | 19.61 ± 0.04 | H I | 21.17 ± 0.10 |
| H ₂ ($J = 1$) | 19.62 ± 0.03 | D I | 16.16 ± 0.12 |
| H ₂ ($J = 2$) | 18.15 ± 0.25 | O I | 17.93 ± 0.10 |
| H ₂ ($J = 3$) | 17.32 ± 0.30 | N I | 17.10 ± 0.04 |
| H ₂ ($J = 4$) | 15.44 ± 0.08 | Fe II | 15.22 ± 0.04 |
| H ₂ ($J = 5$) | 14.81 ± 0.06 | P II | 14.58 ± 0.07 |
| H ₂ ($J = 6$) | 13.60 ± 0.10 | C I | 14.1: |
| H ₂ (total) | 19.92 ± 0.04 | C I* | 13.7: |
| CO ($J = 0$) | 13.49 ± 0.08 | C I** | 13.2: |
| CO ($J = 1$) | 13.35 ± 0.12 | Ar I | 15.4: |
| CO (total) | 13.73 ± 0.08 | HD (total) | 14.52 ± 0.12 |

^a 2σ error bars. Colons indicate uncertain results.

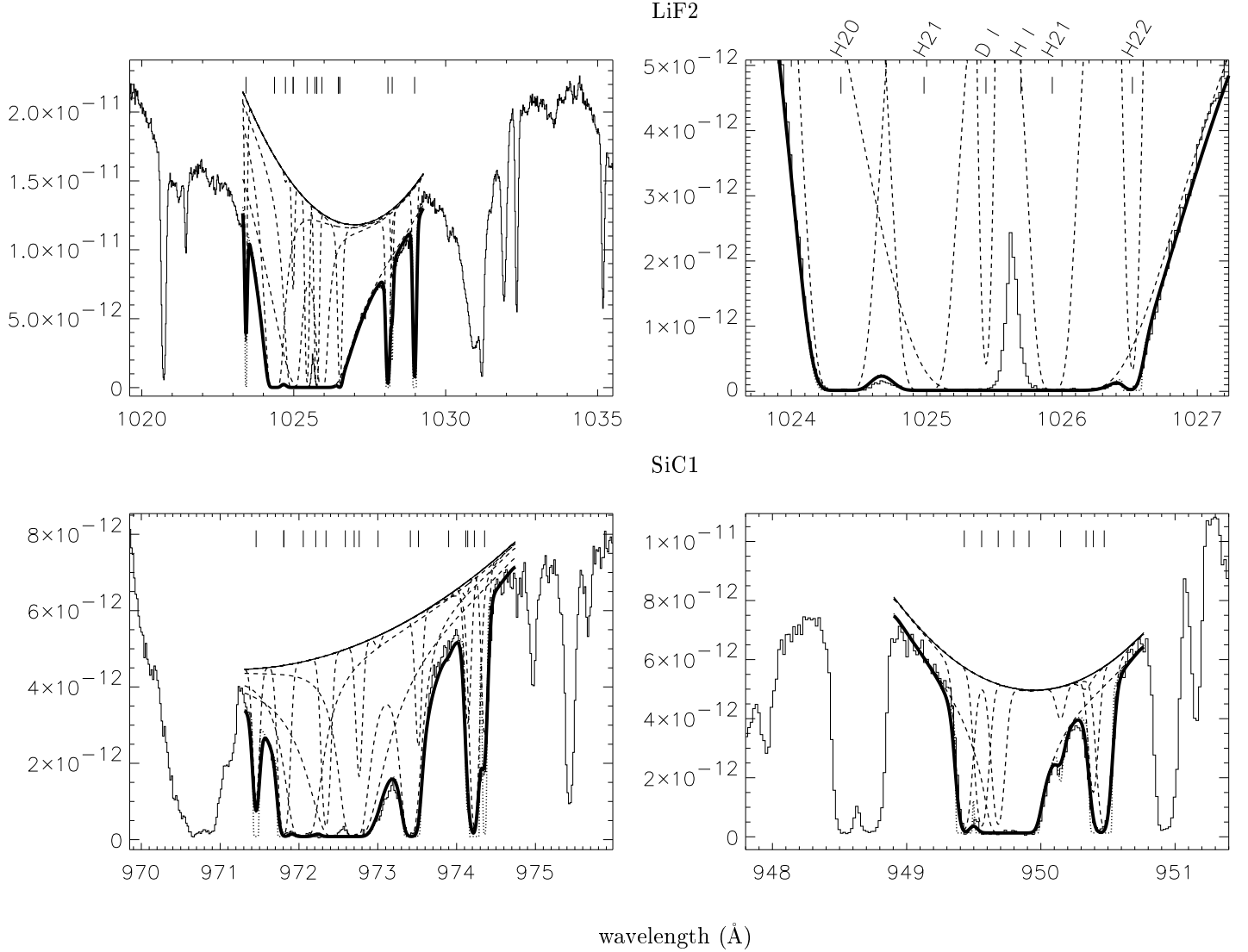


FIG. 11.— Fit of the Ly- β , Ly- γ , and Ly- δ H I lines observed with *FUSE* toward HD 90087. Same conventions as in Fig. 3 but for clarity, the species are not identified at the top of the plots on three of the four panels. The emission lines in the cores of the H I absorptions (near 1025.65 Å and 972.55 Å) are geocoronal. The result is in agreement with the measurement from Ly- α (*IUE*), but the stellar continua are difficult to constrain, especially for Ly- β .

TABLE 4
RATIOS TOWARD HD 90087.

| Ratio | Value ^a |
|--------------------|--------------------------------|
| D/O | $(1.7 \pm 0.7) \times 10^{-2}$ |
| D/N | $(1.1 \pm 0.4) \times 10^{-1}$ |
| D/H | $(9.8 \pm 3.8) \times 10^{-6}$ |
| O/H | $(5.8 \pm 2.0) \times 10^{-4}$ |
| N/H | $(8.5 \pm 2.2) \times 10^{-5}$ |
| CO/H ₂ | $(6.5 \pm 1.4) \times 10^{-7}$ |
| $f(\text{H}_2)$ | $10.1 \pm 2.6 \%$ |
| HD/D I | $2.3 \pm 1.0 \%$ |
| HD/2H ₂ | $(2.0 \pm 0.6) \times 10^{-6}$ |

^a 2σ error bars.

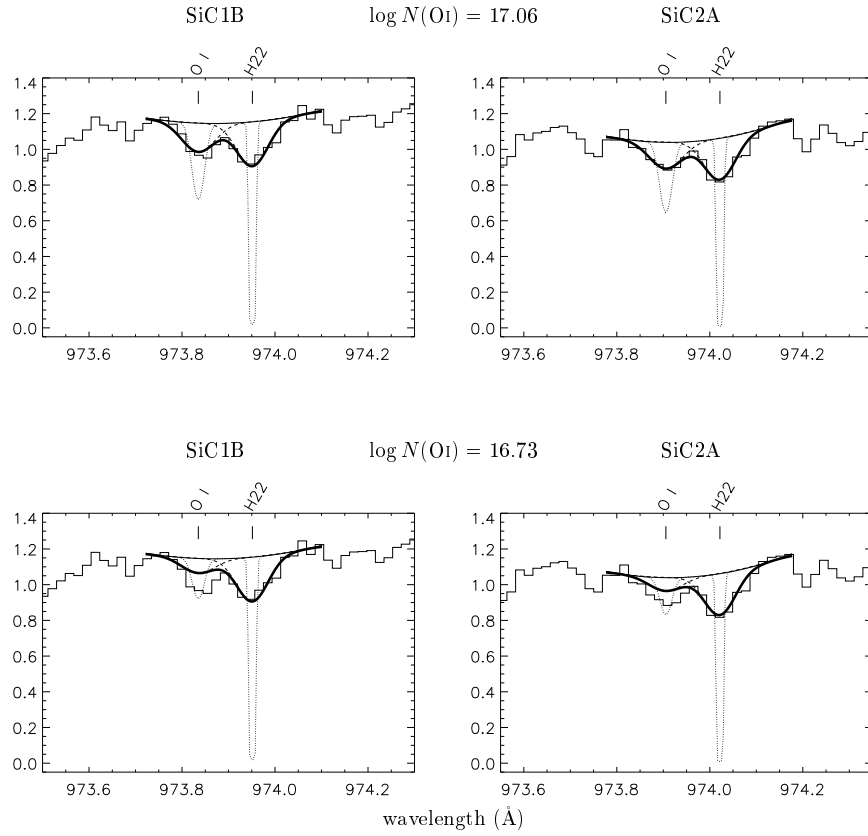


FIG. 12.— Fits of the $\lambda 974.07 \text{ \AA}$ O I line toward Feige 110. Same conventions as in Fig. 3. The Y-axis is flux in $10^{-11} \text{ erg/cm}^2/\text{s}/\text{\AA}$. The upper panel shows our fit of the SiC1B and SiC2A data. The lower panel shows the fit of the same data assuming the O I column density reported by Friedman et al. (2002). The $\lambda 974.07 \text{ \AA}$ line suggests this early $N(\text{O I})$ measurement was underestimated by a factor ~ 2 .

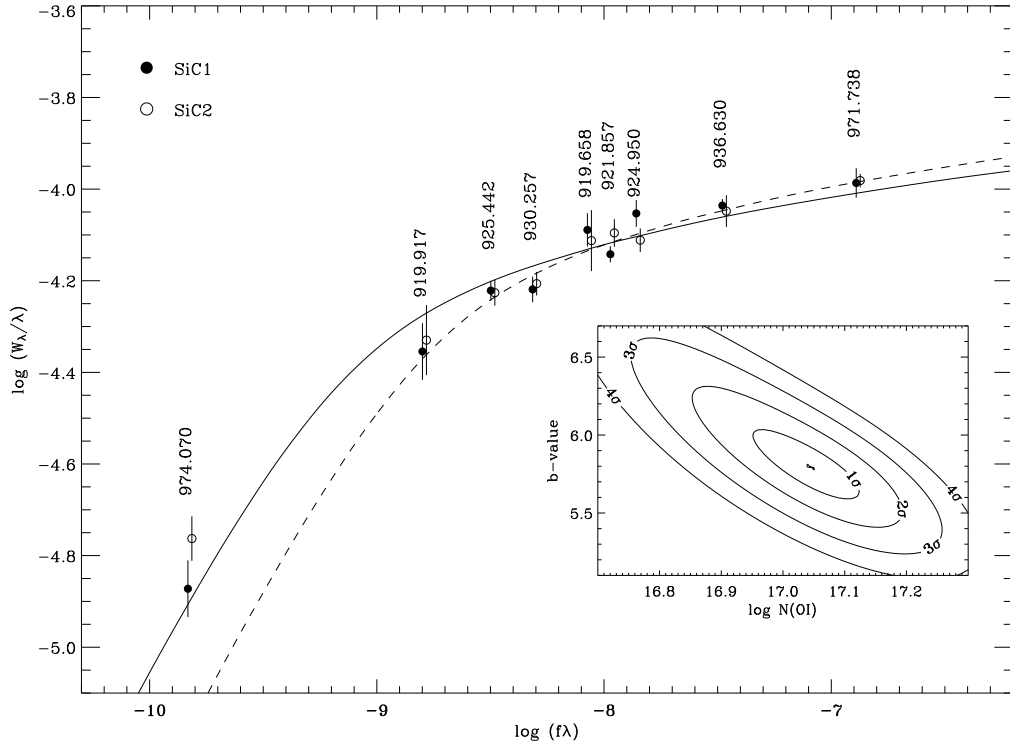


FIG. 13.— The single component, Gaussian curve-of-growth for O I toward Feige 110. The best fit solution (solid line) is $\log N(\text{O I}) = 17.04^{+0.15}_{-0.18}$ and $b = 5.80^{+0.51}_{-0.39}$. The solution if the $\lambda 974 \text{ \AA}$ line is not included (dashed line) is 16.73 ± 0.10 and $b = 6.58 \pm 0.35$. The inset show the $\log(N)/b$ -value error contours. For clarity, at each wavelength the data points derived from each of the *FUSE* channels have been slightly separated. Including saturated lines might lead to erroneous column density measurements and underestimations of error bars.

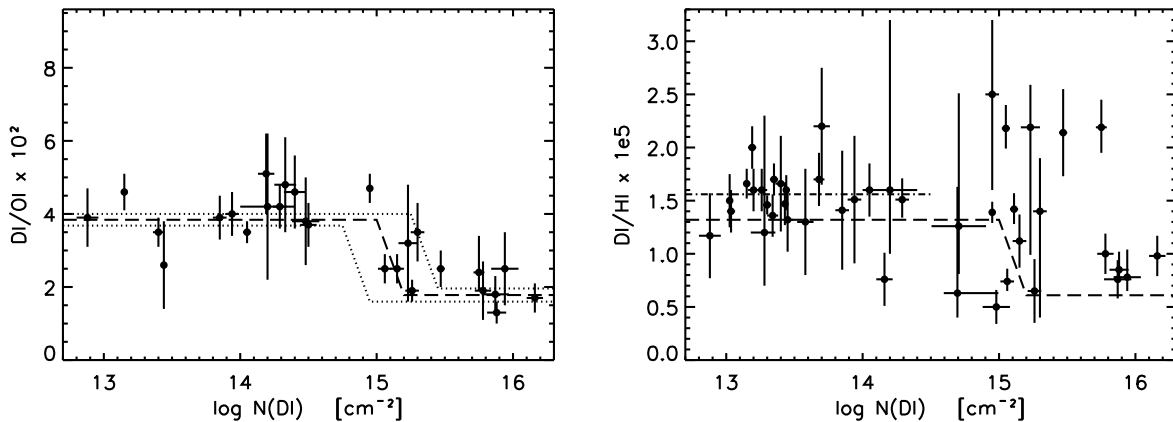


FIG. 14.— D/O (left) and D/H (right) as a function of $\log N(\text{D I})$. The y -axes of the two plots are scaled to the same size, assuming $\text{O}/\text{H} = 3.43 \times 10^{-4}$ (Meyer 2001). The D/O plot (left) shows a simple, bimodal picture (dashed line, with dotted error bars): there are a local and a distant D/O ratio, respectively $(3.84 \pm 0.16) \times 10^{-2}$ and $(1.78 \pm 0.18) \times 10^{-2}$, with a transition around $\log N(\text{D I}) = 15 - 15.3$. The extension of the transition area is not well constrained with the currently available dataset. The D/H plot (right) shows a less simple, more scattered picture, which doesn't fit with the D/O bimodal picture (dashed line, over-plotted here for comparison). The D/O ratios measured on distant sight lines ($\log N(\text{D I}) > 15$) are all low, whereas there are targets in the same column density range which present high D/H ratios. Note that the local D/H ratio $(1.56 \pm 0.04) \times 10^{-5}$ (Wood et al. 2004, dashed-dotted line) is significantly higher the local D/H ratio inferred from D/O measurements (see Hébrard & Moos 2003). All the error bars plotted here are 1σ .